Monitoring cancer cell proliferation through etched optical fiber sensor

C. L. Gomez[a,*], L. Hernández Aragón[b], P. Zaca-Morán[a], F. Galindo Ramírez[b], and O. Zaca Moran[c]

[a]*Instituto de Ciencias, Benemérita Universidad Autónoma de Puebla, 72050, Puebla, México,*

[b]*Instituto de Fisiología, Benemérita Universidad Autónoma de Puebla, 72050, Puebla, México,*

[c]*Instituto Politécnico Nacional, Centro de Investigación en Biotecnología Aplicada, Ex-Hacienda de San Juan Molino, Km 1.5 de la Carretera Estatal Santa Inés, Tecuexcomac-Tepetitla, Tepetitla, 90700, Tlaxcala, México,*

[*]*e-mail: celia.gomez@correo.buap.mx*

Received 23 June 2025; accepted 6 October 2025

In the present work, the real-time monitoring of murine lung cancer cell line proliferation using the evanescent field generated in an etched optical fiber is presented. The sensor was fabricated by removing 1 cm of the cladding from a single-mode optical fiber using hydrofluoric acid, exposing the 10 μm diameter core. Cell proliferation was monitored using a continuous-wave 1550 nm infrared laser by monitoring power transmission variations in the cell culture medium. The etched fiber detects transmission variations starting at approximately 2.1×10^5 cells/mL and that the sensor operates stably over the 24 to 96 h interval, during which the refractive index of the supernatant $(1.298 - 1.335)$ remains well below the refractive index of the fiber core (≈ 1.452). The cell proliferation results obtained with this technique were compared with those from an automatic quantifier, showing an inverse relationship between cell proliferation and laser transmission. The lung cancer cells were studied over a concentration range from 2.1×10^5 to 51.1×10^5 cells/mL. The present study validates the sensor's effectiveness by correlating light transmission with cell density and refractive index changes. This detection method can be used for rapid cell proliferation analysis in laboratories and hospitals, as well as for studying properties such as refractive index and penetration depth of biological media, making these sensors ideal for studying biological compounds in biochemistry and biomedicine.

Keywords: Cell proliferation; etched optical fiber; Sensor; infrared lase; refractive index.

DOI: https://doi.org/10.31349/RevMexFis.72.021301

1. Introduction

The study of cell proliferation is crucial for tissue growth and regeneration in multicellular organisms, significantly impacting various scientific and medical fields. Understanding and monitoring cell proliferation enables a deeper comprehension of fundamental biological processes and the effectiveness of medical and pharmacological treatments. It also facilitates early detection and treatment of pathological anomalies, optimizes cell cultures in biotechnological applications, personalizes medical treatments, and contributes to the advancement of scientific knowledge and research [1-4]. The primary methods for measuring cell proliferation can be divided into four groups: metabolic activity assays, cell proliferation markers, adenosine triphosphate (ATP) concentration measurement, and deoxyribonucleic acid (DNA) synthesis evaluation [5-10]; however, cell growth monitoring can also be evaluated through microscopy or by using techniques that analyze electrical parameters, such as phase contrast microscopy for morphological observations [11-13], flow cytometry, and electrical impedance for tracking adherence [14-17]. On the other hand, photonic measurement devices have been widely used for the quantification of physicochemical parameters because they are highly efficient as transducers, have rapid response times, offer flexibility, and consume low amounts of energy [18-21]. Arif E. Cetin *et al*. [22] developed a functional plasmonic assay platform that can accurately measure cell mass and dynamic changes in real-time for adherent cells. The device has the capability to determine the growth rates of individual cells within 10 min, allowing for the mapping of growth profiles of cell populations over short time intervals. With this device, they were able to determine the kinetics of cell growth in small samples. However, these devices are difficult to standardize and require mechanical accessories to operate. Devices based on the evanescent field phenomenon are especially sensitive and rely on the interaction of light with substances near the surface of the fiber [23-25]. Among them, fiber optic sensors that expose the evanescent field beyond the fiber surface stand out. These sensors offer advantages such as label-free detection, small sample size, real-time response, and low cost [26]. Mohammad *et al*. [27] reported a single-mode tapered fiber optic biosensor for real-time monitoring of *Escherichia coli* (*E. coli K-12*) growth in an aqueous medium. The tapered fibers, with a waist diameter of 6 to 7 μm and a length of 3 mm, were fabricated using the flame-brushing method. Bacteria were immobilized on the surface of the fiber optic using poly-L-lysine. The reported results showed that the specific growth rate measured with the biosensor was approximately 0.17 ∓ 0.01 cells/h over a period of 1.6 h at room temperature. When the bacteria grew on the fiber, the fiber optic biosensor exhibited significant transmission changes at 1558 nm,

which is proportional to the variation in bacterial concentration. Thus, they inferred that the transmission through the fiber decreased with the increase in the average surface density of the bacteria on the tapered fiber. The increase in average bacterial density changes the refractive index of the tapered section.

Ragini Sinhgh *et al*. [28] proposed a compact, portable, label-free, and ultrasensitive sensor for detecting cancer cells based on a multi-core fiber (MCF) consisting of seven cores arranged in a hexagonal shape and spliced to a single-mode fiber (SMF). In this case, cytodetection based on Localized Surface Plasmon Resonance (LSPR) is used for the efficient detection of different types of cancer cells. The structure of the proposed sensor was etched in a controlled manner to enhance the evanescent waves (EWs) and mode coupling between the MCF cores. The etched MCF-based LSPR sensor has high refractive index sensitivity (RIS). To further increase the sensor's sensitivity, they immobilized various nanomaterials (NMs) such as gold nanoparticles (AuNPs), graphene oxide (GO), and copper oxide nanoflowers (CuO-NFs). The AuNPs enhance sensitivity using LSPR, while GO and CuO-NFs help increase the sensor's biocompatibility. The developed sensor was coated with 2-deoxy-D-glucose (2-DG) on the NMs, which are specific for cancer cell detection. In their research, they detected various cancer cell lines such as HepG2, Hepa 1-6, MCF-7, A549, and normal cell lines such as NCF and LO2. They carried out tests on selectivity, reuse, anti-interference capability, and the involvement of the GLUT receptor in detection. The proposed etched sensor is ultrasensitive for detecting cell lines HepG2, Hepa 1-6, A549, MCF-7, LO2, and NCF with a limit of detection (LoD) of 3, 2, 2, 2, 4, and 10 cells/mL, respectively, in the linear range of 1×10^2 - 1×10^6 cells/mL. The drawback of this type of sensor is that it uses a multi-core fiber whose light transmission efficiency is lower compared to a single-mode fiber, and its use is limited to a single measurement per event.

In the present work, a novel method for real-time monitoring of murine lung cancer cell line proliferation using an etched optical fiber through the evanescent field generated in the longitudinal section of the fiber core is presented. Cell proliferation quantification was obtained by measuring power transmission variations of a 1550 nm infrared laser. This detection method has the potential to be used for rapid cell proliferation analysis in laboratories and hospitals. The advantages of this kind of technique used in cellular biology to study cell proliferation, cell concentration changes and interfacial molecular events are that it is independent of high complexity and high fabrication costs, in addition to compact size and freedom of electromagnetic interference. For this purpose, a ~ 1 cm segment of single-mode fiber (SMF-28) was chemically etched to expose 8 μm of the core. The setup was sterilized to allow contact with LP07 cell cultures. Optical transmission was continuously monitored using a 1550 nm laser for 96 h, and the results were correlated with automatic cell counting and the refractive index of the supernatant using calibration curves.

2. Methodology

2.1. Theoretical background

Optical fiber sensors based on evanescent wave absorption detect variations in transmitted power when the guided mode interacts with an external medium whose refractive index n_{sol} differs from the core index n_{core}. Removing the cladding and exposing the core causes part of the fundamental mode's energy to leak into the surrounding medium as an evanescent field. This leaked energy is known as the cladding power P_{loss} (also called P_{clad}) and corresponds to the fraction of optical power that leaves the core [29]. To characterize the phenomenon, we denote by P_{in} is the optical power injected into the fiber and P_{out} the optical power measurement at the output; the difference between them [29],

$$P_{\text{loss}} = P_{\text{in}} - P_{\text{out}}, \tag{1}$$

were P_{loss} represents the optical power lost though evanescent interaction whit the external medium, and the fractional evanescent power F is defined as the ratio of lost power to input power [29]:

$$F = \frac{P_{\text{loss}}}{P_{\text{in}}}. \tag{2}$$

Under the weakly guiding approximation for the fundamental mode of a single-mode fiber with core radius r and operating at wavelength λ, this fractional evanescent power F can be estimated analytically as [29]

$$F = \frac{4\sqrt{2}}{3} \frac{\lambda}{2\pi r \sqrt{(n_{\text{core}}^2 - n_{\text{sol}}^2)}}. \tag{3}$$

This expression is dimensionless because λ/r is a ratio of lengths and $P_{\text{loss}}/P_{\text{in}}$ is a ratio of powers. The factor $4\sqrt{2}/3$ arises from modal analysis in weakly guiding fibers. In our experiments, n_{sol} refers to the refractive index of the culture supernatant surrounding the fiber and varies as the cell population grows.

In practice, instead of solving Eq. (3) analytically for n_{sol}, we use a calibration curve $T(n)$ obtained with reference solutions of known refractive index (*e.g.* sucrose solutions). This curve allows us to map changes in transmitted power directly to refractive index values without inserting power terms into the denominator, which avoids dimensional errors and improves measurement traceability.

Finally, the penetration depth of the evanescent field into the medium is given by [29]

$$D_P = \frac{\lambda}{2\pi n_{\text{core}} \sqrt{\sin^2 \theta_i - (\frac{n_{\text{sol}}}{n_{\text{core}}})^2}}, \tag{4}$$

where θ_i is the internal incidence angle at the core/cladding interface (near the critical angle). This depth (typically a few tenths of a micrometer) determines the volume of supernatant interacting with the evanescent field and therefore influences sensor sensitivity.

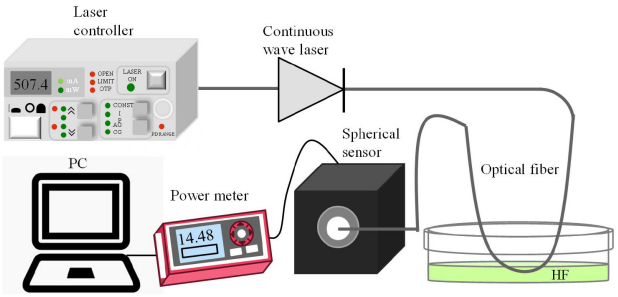

FIGURE 1. Experimental setup for chemical etching of the optical fiber with HF.

2.2. Preparation of the etched optical fiber

The fabrication of the sensing device was carried out removing the cladding from a single-mode optical fiber (SMF-28), exposing the 8 μm core using the chemical etching method with hydrofluoric acid (HF) as reported by Zaca-Morán *et al*. [30]. The chemical etching process involved removing approximately 1 cm of plastic coating from the fiber using a fiber stripping tool (Fiber Stripping Tool, T06S13). The bare optical fiber was placed in a 10 cm diameter Petri dish, with one end connected to a laser system and the other end to a power sensor to monitor the transmitted radiation. The cladding was removed by immersing the fiber in HF $48.0-51.0\%$ (JT BAKER, 9560-06) at room temperature for 35 min. After the process, the reduced fiber was thoroughly cleaned with triple-distilled water (COPAIN) to eliminate any HF residue.

Figure 1 shows the experimental setup for the chemical etching of the optical fiber, which includes a continuous-wave 1550 nm emission laser with fiber optic output (Thorlabs, model FPL1009S). A digital power meter (Thorlabs, model PM100D) was used to monitor the system output, complemented by an InGaAs integrating sphere sensor (Thorlabs, model S145C), operating in the wavelength range from 800 to 1700 nm. The transmission measurement results were acquired using a computer with the PM100D Utility program for subsequent analysis.

2.3. Culture of murine lung cancer LP07 cells

Cells from the LP07 murine lung tumor cell line were used and seeded in 10 cm diameter Petri dishes with Minimum Essential Media (MEM, Gibco), supplemented with 10% fetal bovine serum (FBS, Gibco) and 1X antibiotic-antimycotic (Gibco). Five Petri dishes were seeded with the same cell density of approximately 125000 ∓ 17677.7 total cells. Cell growth was carried out in an incubator (ThermoScientific, model HERAcell 150i) with a 5% carbon dioxide (CO_2) atmosphere at a temperature of $37°$C. An automatic cell counter (Countess III, Invitrogen) was used for automatic cell quantification by triplicate values for each Petri dish every 24 h, from cell seeding until 96 h, in parallel with the real-time monitoring proliferation cell. The cell culture supernatants were analyzed every 24 h using Fourier Transform Infrared Spectroscopy (FTIR) in the range of 4000 to 400 cm^{-1} with a spectrophotometer (Bruker, Vertex 70) in attenuated total reflection (ATR) mode. The baseline used was the ATR crystal, on which 3 μL of supernatant was dried at room temperature. These data were then correlated with real-time cell proliferation.

2.4. Etched optical fiber sensor

The experimental setup and the reduced optical fiber were sterilized for 24 h using an ultraviolet (UV) lamp to maintain sterile conditions within the incubator before monitoring cell proliferation. One of the Petri dishes contained the reduced optical fiber, while the other four were used for automatic cell quantification; monitoring began 24 h after cell seeding. The medium containing dead cells or cell debris from the seeding process was removed before starting the real-time monitoring, as these could interfere with the sensitivity of the reduced fiber when placed on it. The experimental setup for studying cell proliferation is shown in Fig. 2. A continuous wave laser (Thorlabs, model FPL1009S) emitting at 1550 nm was used, controlled by a current controller (Thorlabs, model ITC510). Finally, to carry out proliferation monitoring, a maximum output power of 50 mW was used with an applied current of 400 mA.

According to the experimental setup, the evanescent wave generated will interact with the cell culture solution placed in the incubator. The power meter will monitor changes in laser transmission and take measurements every second for a continuous period of 72 h.

3. Results and discussion

The results obtained from the reduction process through chemical etching are presented in Fig. 3, where it can be observed that the transmitted power remains constant for up to 30 min. Subsequently, the transmitted power along the optical fiber begins to decrease abruptly. Since the chemical attack using HF is a process that linearly etches the optical fiber [30], and given that the total time for the first fiber to fully etch was 37.5 min, the etching rate was determined to be 3.24 μm/min. Therefore, to completely remove the cladding of the optical fiber, it was necessary to leave it in the chemical

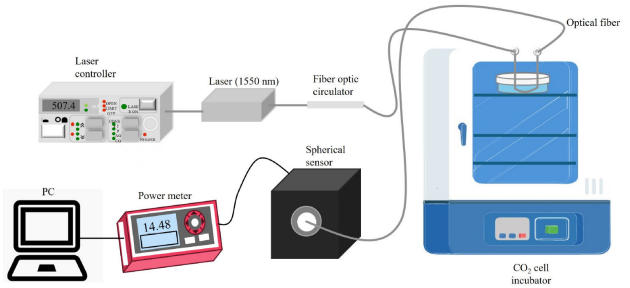

FIGURE 2. Experimental setup to monitor cell proliferation in real time.

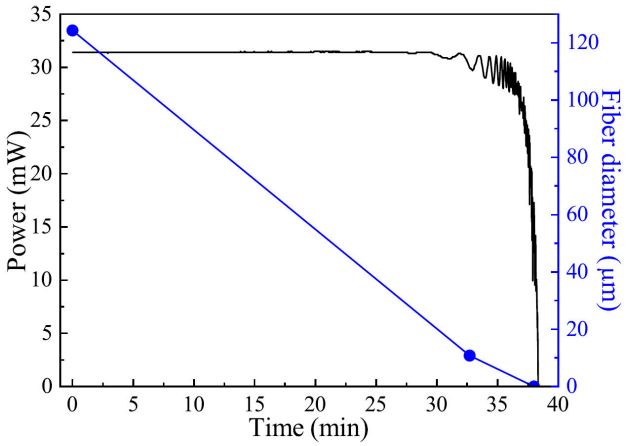

FIGURE 3. Optical fiber transmission during chemical etching with HF.

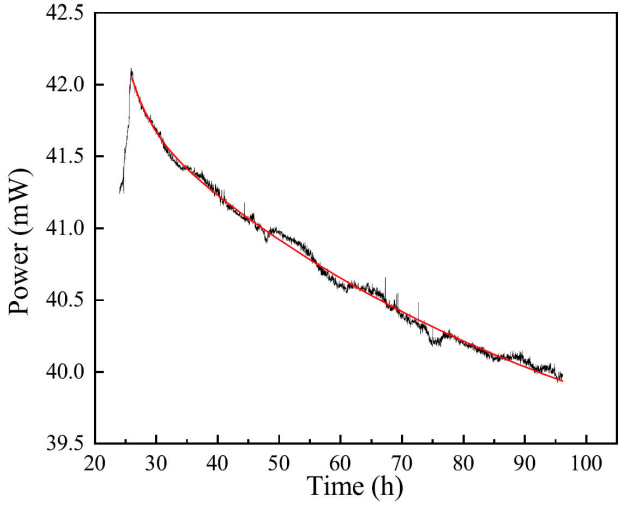

FIGURE 4. Laser output power in the fiber reduced during 72 h continuous of cell proliferation. The red line indicates a fitting of experimental data.

etching with HF for 33 min to achieve an optical fiber with a reduced diameter of approximately 10 μm, which is close to the core diameter.

The results of the real-time evaluation of cell proliferation using the reduced optical fiber are presented in Fig. 4. This figure shows the dependence of laser output power on the elapsed time during the proliferation of murine lung cancer LP07 cells over a continuous period of 72 h after the seeding cells. As time increased, the transmitted power through the culture medium decreased over 72 h of proliferation. This result is attributed to the sensor being in contact with a denser medium due to a higher concentration of cells and cellular metabolism products, as the release of factors that promote tumor growth, such as vascular endothelial growth factor (VEGF), which has been quantified in the culture medium of HeLa cells (Henrietta Lacks' cervical carcinoma) by X. Li *et al*. [31] and J. Ko *et al*. [32]. In the other hand, Fig. 5 also shows an increase in laser output power during the first 2 h, which is suggested to be due to the consumption of nutrients in the culture medium, such as glucose, amino acids, free

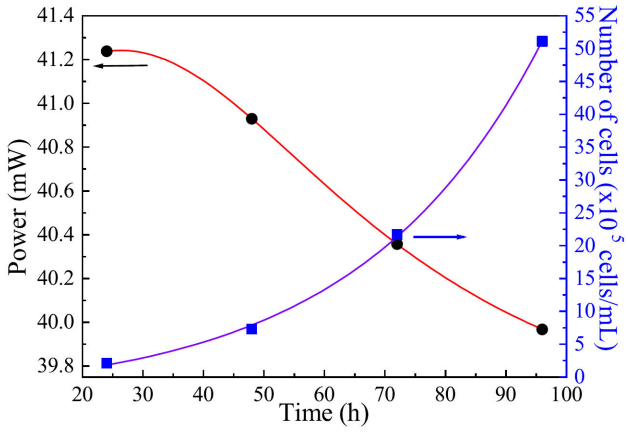

FIGURE 5. Laser power output and the number of cells as a function of proliferation time.

fatty acids, growth factors, or oxygen; since it has been observed that as cells grow, they initially consume the necessary nutrients present in the medium to start their growth [33,34]. The increase at the beginning of the monitoring, fresh culture medium was added, so the presence of these nutrients was higher, but as time passes, the nutrients are gradually consumed by the cells.

In Fig. 5, the laser output power is correlated with the number of automatically quantified cells every 24 h. According to the cell quantification, it was observed that cell proliferation has an increase of $2.1 * 10^5$, $7.3 * 10^5$, $21.7 * 10^5$, and $51.1 * 10^5$ cells/mL at 24, 48, 72, and 96 h, respectively. There was more significant cell growth between 72 and 96 h, according to the phase of cell growth and it is worth noting that LP07 cell line proliferates at a slow rate [35]. The number of cells is inversely proportional with quantified data in the output power; this is attributed to the evanescent field resulting from the culture medium interacting with the etched fiber. It is important to mention that all the experimental data of the optical properties were fitted with a Lorentzian function (red solid line) with a goodness of fit of 0.99754, and for the cell proliferation an exponential decay function (blue solid line) was used to fit the experimental data obtaining a 0.99961 goodness of fit.

To correlate the quantified data in the output power the FTIR spectra of the supernatants were obtained from the cell cultures at 24, 48, 72, and 96 h and are shown in Fig. 6. The spectral bands around 3200 and 3500 cm^{-1}, which are related to OH functional groups; 2900 cm^{-1}, associated with CH functional groups; as well as 1630 and 1540 cm^{-1}, related to Amide I and II functional groups, respectively, were observed. Additionally, bands at 1450 and 1400 cm^{-1} related to proteins, and between 1200 and 1083 cm^{-1}, identified with nucleic acids [36], were also present. All functional groups identified are the main components of the culture medium constituted by BSA and MEM [37,38]. The analysis of the amide I-related band can be associated with

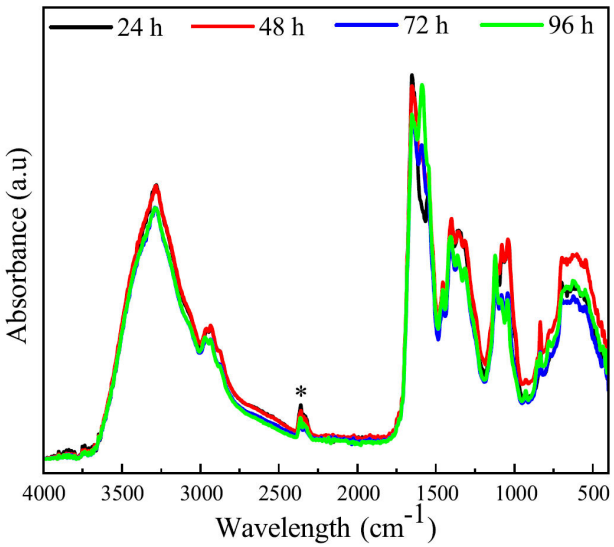

FIGURE 6. FTIR spectra of the supernatants of murine lung cancer cells at 24, 48, 72, and 96 h. The $*$ mark refers to the CO_2 present at the time of analyzing the samples.

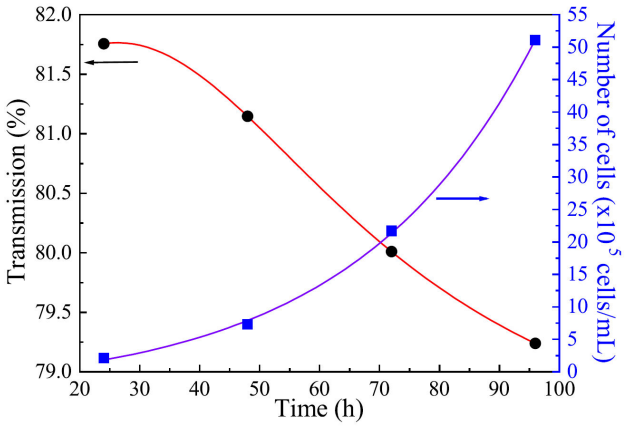

FIGURE 7. Etched optical fiber transmission and the number of cells as a function of proliferation time.

a greater number of cells, because as the proliferation time increases, the intensity of this band decreases.

Figure 7, shows the transmission of the etched fiber in contact with the cell culture as a function of time. It is observed that the transmission decreased as the proliferation time increased, indicating that the transmission of the sensor is inversely proportional to cell confluence. These changes in transmission through the etched fiber in contact with the cell culture measure the change in evanescent field absorption [27].

The refractive index of the cell culture was calculated using Eq. (3), with values ranging between 1.298 and 1.332 (Fig. 8) over the 72 h of cell proliferation. It was observed that refractive index increased as the number of cells increased, indicating a direct relationship between these two parameters. Under suitable conditions, the growth of the cell population in the medium surrounding the etched fiber increases the average surface density of the cells, consequently increasing the refractive index of the reduced region [27].

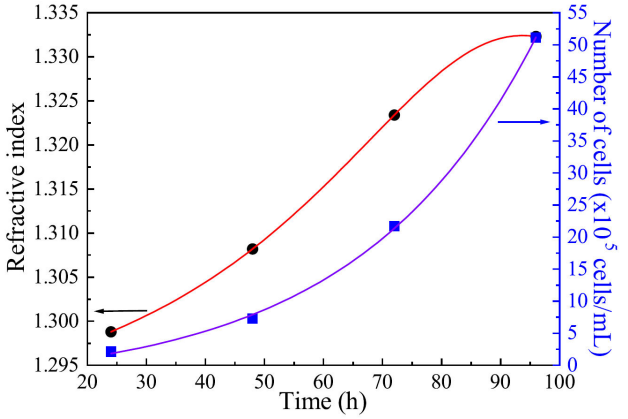

FIGURE 8. Dependence of the refractive index and the number of cells on proliferation time.

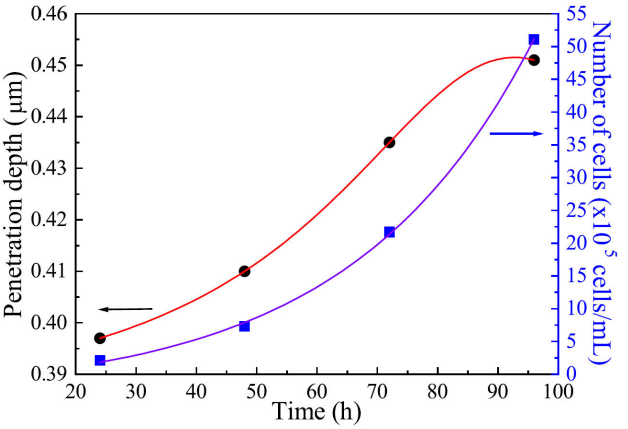

FIGURE 9. Penetration depth of light in an optical fiber and the number of cells as functions of proliferation time.

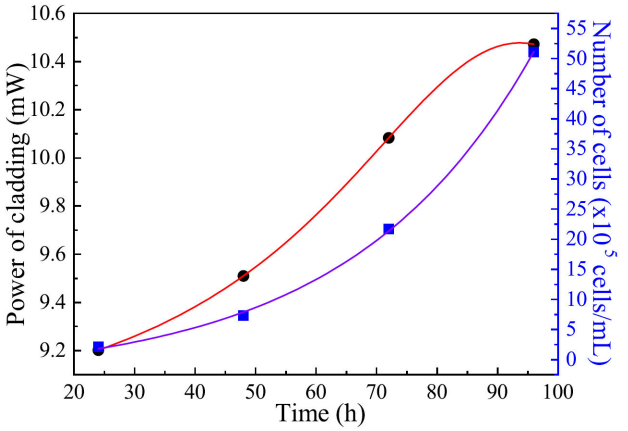

FIGURE 10. Dependence of the calculated power of cladding on the medium and the number of cells on proliferation time.

In Fig. 9 it was observed that the penetration depth of the evanescent field into the cell culture in contact with the etched fiber increased as the number of cells increased, calculated using Eq. (4). The fact that the penetration depth increases is

because the sensitivity of the sensor improves, as a large penetration depth of an evanescent wave is key to the successful development of fiber optic evanescent wave sensors [39].

The power of the evanescent wave interacting with the solution was calculated using Eq. (1) as shown in Fig. 10, where the power increased as the number of cells in the culture grew.

The exposure of the etched fiber to the cell culture medium leads to changes in its optical properties, as observed in this study. These changes in optical properties affect the evanescent field, resulting in variations in the optical performance of the sensing device [27].

4. Conclusion

In this study an optical fiber sensor was developed and used for real-time monitoring of cell proliferation in a murine lung cancer cell line. The results showed that the use of the evanescent field generated in the fiber allowed for the detection of changes in the light transmission as the cells proliferated, with a decrease in laser output power, indicating an inverse relationship between cell proliferation and optical transmission. Additionally, it was determined that the refractive index of the culture medium increased as cell density grew, suggesting the sensor's ability to detect changes in the optical properties of biological media. This sensor not only provides a correlation between light transmission, cell quantity, and the refractive index but also stands out for its low cost and real-time measurement capability. These results suggest that the sensor has potential for biomedical and biochemical applications, as well as for studying molecular interactions in biological media.

Acknowledgments

This work was supported by SECIHTI (formerly CONAHCYT) under grant agreements no. BPPAIM-2022090615173476 9-3682852, CBF-2025-G-1054 and CF-2023-G-1080.

1. E. González-Gualda, A. G. Baker, L. Fruk, and D. Muñoz-Espín, A guide to assessing cellular senescence in vitro and in vivo, *FEBS J.* **288** (2021) 56, https://doi.org/10.1111/febs.15570.
2. S. Patergnani *et al.*, Various aspects of calcium signaling in the regulation of apoptosis, autophagy, cell proliferation, and cancer, *Int. J. Mol. Sci.* **21** (2020) 8323, https://doi.org/10.3390/ijms21218323.
3. G. N. Somero, The cellular stress response and temperature: Function, regulation, and evolution, Journal of Experimental Zoology Part A: *Ecological and Integrative Physiology*, **333** (2020) 379, https://doi.org/10.1002/jez.2344.
4. J. Zhu and C. B. Thompson, Metabolic regulation of cell growth and proliferation, *Nat. Rev. Mol. Cell. Biol.* **20** (2019) 436, https://doi.org/10.1038/s41580-019-0123-5.
5. F. J. Hartmann *et al.*, Single-cell metabolic profiling of human cytotoxic T cells, *Nat Biotechnol.* **39** (2021) 186, https://doi:10.1038/s41587-020-0651-8.
6. M. Joannidis *et al.*, Use of cell cycle arrest biomarkers in conjunction with classical markers of acute kidney injury, *Crit Care Med.* **47** (2019) e820, https://doi.org/10.1097%2FCCM.0000000000003907.
7. S. Kamiloglu, G. Sari, T. Ozdal, and E. Capanoglu, Guidelines for cell viability assays, *Food Frontiers* **1** (2020) 332, https://doi.org/10.1002/fft2.44.
8. S. Minchin and J. Lodge, Understanding biochemistry: structure and function of nucleic acids, *Essays Biochem* **63** (2019) 433, https://doi.org/10.1042/EBC20180038.
9. D. Samanta, S. B. Ebrahimi, and C. A. Mirkin, Nucleic-acid structures as intracellular probes for live cells, *Advanced Materials* **32** (2020) 1901743, https://doi.org/10.1002/adma.201901743.
10. D. Zhao *et al.*, Rapid and specific imaging of extracellular signaling molecule adenosine triphosphate with a self-phosphorylating DNAzyme, *J. Am. Chem. Soc.* **143** (2021) 15084, https://doi.org/10.1021/jacs.1c04925.
11. V. H. Blahnova, J. Dankova, M. Rampichova, and E. Filova, Combinations of growth factors for human mesenchymal stem cell proliferation and osteogenic differentiation, *Bone Joint J.* **9** (2020) 412, https://doi:10.1302/2046-3758.97.BJR-2019-0183.R2.
12. Z. Kong, X. Zhu, S. Zhang, J. Wu, and Y. Luo, Phase contrast microscopy of living cells within the whole lens: spatial correlations and morphological dynamics, *Mol Vis.* **18** (2012) 2165, http://www.molvis.org/molvis/v18/a228.
13. K. Thirusittampalam, M. J. Hossain, O. Ghita, and P. F. Whelan, A novel framework for cellular tracking and mitosis detection in dense phase contrast microscopy images, *IEEE J BIOMED HEALTH* **17** (2013) 642, https://doi.org/10.1109/titb.2012.2228663.
14. J. Chen, C. Xue, Y. Zhao, D. Chen, M.-H. Wu, and J. Wang, Microfluidic impedance flow cytometry enabling high-throughput single-cell electrical property characterization, *Int. J. Mol. Sci.* **16** (2015) 9804, https://doi.org/10.3390/ijms16059804.
15. H. Daguerre, M. Solsona, J. Cottet, M. Gauthier, P. Renaud, and A. Bolopion, Positional dependence of particles and cells in microfluidic electrical impedance flow cytometry: Origin, challenges and opportunities, *Lab Chip* **20** (2020) 3665, https://doi.org/10.1039/D0LC00616E.
16. F. Gökçe, P. S. Ravaynia, M. M. Modena, and A. Hierlemann, What is the future of electrical impedance spectroscopy in flow cytometry?, *Biomicrofluidics* **15** (2021) 061302, https://doi.org/10.1063/5.0073457.

17. Y. Xu, X. Xie, Y. Duan, L. Wang, Z. Cheng, and J. Cheng, A review of impedance measurements of whole cells, *Biosensors and Bioelectronics* **77** (2016) 824, https://doi.org/10.1016/j.bios.2015.10.027.

18. M. A. Mollah, R. J. Usha, S. Tasnim, and K. Ahmed, Detection of cancer affected cell using Sagnac interferometer based photonic crystal fiber refractive index sensor, *Opt Quant Electron* **52** (2020) 1, https://doi.org/10.1007/s11082-020-02542-y.

19. M. Ochoa, J. F. Algorri, P. Roldán-Varona, L. Rodríguez-Cobo, and J. M. López-Higuera, Recent advances in biomedical photonic sensors: A focus on optical-fibre-based sensing, *Sensors* **21** (2021) 6469, https://doi.org/10.3390/s21196469.

20. A. Venketeswaran *et al*., Recent advances in machine learning for fiber optic sensor applications, *Advanced Intelligent Systems* **4** (2022) 2100067, https://doi.org/10.1002/aisy.202100067.

21. Y. Zhao, X.-g. Hu, S. Hu, and Y. Peng, Applications of fiber-optic biochemical sensor in microfluidic chips: A review, *Biosensors and Bioelectronics* **166**, (2020), 112447, https://doi.org/10.1016/j.bios.2020.112447.

22. A. E. Cetin, S. N. Topkaya, O. Yalcin-Ozuysal, and A. Khademhosseini, Refractive Index Sensing for Measuring Single Cell Growth, *ACS Nano* **15** (2021) 10710, https://doi.org/10.1021/acsnano.1c04031.

23. L. Jiao, N. Zhong, X. Zhao, S. Ma, X. Fu, and D. Dong, Recent advances in fiber-optic evanescent wave sensors for monitoring organic and inorganic pollutants in water, *Trends Anal. Chem.* **127** (2020) 115892, https://doi.org/10.1016/j.trac.2020.115892.

24. A. J. Y. Tan, S. M. Ng, P. R. Stoddart, and H. S. Chua, Theoretical model and design considerations of U-shaped fiber optic sensors: A review, *IEEE Sensors Journal* **20** (2020) 14578, https://doi.org/10.1109/JSEN.2020.3011173.

25. P. Tao *et al*., Fiber optic SERS sensor with silver nanocubes attached based on evanescent wave for detecting pesticide residues, *ACS Appl. Mater. Interfaces* **15** (2023) 30998, https://doi.org/10.1021/acsami.3c04059.

26. S. Mena, M. Morant, J. Hurtado, and R. Llorente, Tapered Fibre Optic Biosensor (TFOBS) by Optically Controlled Etching for Label-Free Glucose Concentration Monitoring - Biomedical, *Optics* (2018) 166, https://doi:10.5220/0006556301660173.

27. M. I. Zibaii, A. Kazemi, H. Latifi, M. K. Azar, S. M. Hosseini, and M. H. Ghezelaiagh, Measuring bacterial growth by refractive index tapered fiber optic biosensor, *J. Photochem. Photobiol. B* **101** (2010) 313, https://doi.org/10.1016/j.jphotobiol.2010.07.017.

28. R. Singh *et al*., Etched multicore fiber sensor using copper oxide and gold nanoparticles decorated graphene oxide structure for cancer cells detection, *Biosensors and Bioelectronics* **168** (2020) 112557, https://doi.org/10.1016/j.bios.2020.112557.

29. N. Punjabi, J. Satija, and S. Mukherji, Evanescent wave absorption based fiber-optic sensor-cascading of bend and tapered geometry for enhanced sensitivity, Sensing Technology: Current Status and Future Trends III, Springer, 25-45.

30. P. Zaca-Morán, J. P. Padilla-Martínez, J. M. Pérez-Corte, J. A. Dávila-Pintle, J. G. Ortega-Mendoza, and N. Morales, Etched optical fiber for measuring concentration and refractive index of sucrose solutions by evanescent waves, *Laser Physics* **28** (2018) 116002, https://doi:10.1088/1555-6611/aad846.

31. X. Li, M. Soler *et al*., Plasmonic nanohole array biosensor for label-free and real-time analysis of live cell secretion, *Lab on a Chip* **17** (2017) 2208, https://doi.org/10.1039/C7LC00277G.

32. J. Ko, J. Ham, H. Lee, K. Lee, and W.-G. Koh, Integration of a fiber-based cell culture and biosensing system for monitoring of multiple protein markers secreted from stem cells, *Biosensors and Bioelectronics* **193** (2021) 113531, https://doi.org/10.1016/j.bios.2021.113531.

33. A. Fedi, C. Vitale, P. Giannoni, G. Caluori, and A. Marrella, Biosensors to monitor cell activity in 3D hydrogel-based tissue models, *Sensors* **22** (2022) 1517, https://doi.org/10.3390/s22041517.

34. M. M. Modena, K. Chawla, P. M. Misun, and A. Hierlemann, Smart cell culture systems: Integration of sensors and actuators into microphysiological systems, *ACS chemical biology* **13** (2018) 1767, https://doi.org/10.1021/acschembio.7b01029.

35. A. J. Urtreger *et al*., New murine cell line derived from a spontaneous lung tumor induces paraneoplastic syndromes, *Int. J. Oncol.* **18** (2001) 639, https://doi.org/10.3892/ijo.18.3.639.

36. W. Yang, X. Xiao, J. Tan, and Q. Cai, In situ evaluation of breast cancer cell growth with 3D ATR-FTIR spectroscopy, *Vib. Spectrosc.* **49** (2009) 64, https://doi.org/10.1016/j.vibspec.2008.04.016.

37. X. Yang *et al*., Diagnosis of lung cancer by ATR-FTIR spectroscopy and chemometrics, *Frontiers in Oncology* **11** (2021) 753791, https://doi.org/10.3389%2Ffonc.2021.753791.

38. X. Yang *et al*., Diagnosis of lung cancer by FTIR spectroscopy combined with Raman spectroscopy based on data fusion and wavelet transform, *Front Chem* **10** (2022) 810837, https://doi.org/10.3389%2Ffchem.2022.810837.

39. J. Lu, Z. Chen, F. Pang, and T. Wang, Theoretical analysis of fiber-optic evanescent wave sensors in In 2008 China-Japan Joint Microwave Conference IEEE., (IEEE, 2008) 583, https://doi.org/10.1109/CJMW.2008.4772500.